Quadrature-Error Compensation and Corresponding Effects on the Performance of Fully Decoupled MEMS Gyroscopes

Erdinc Tatar, Said Emre Alper, *Member, IEEE*, and Tayfun Akin

***Abstract*—This paper presents experimental data about the sources of the quadrature error in a fully decoupled microelectromechanical systems gyroscope and demonstrates the extent of performance improvement by the cancellation of this error. Quadrature sources including mass, electrostatic-force, and mechanical-spring imbalances have been compared by FEM simulations, and spring imbalance has been found as the dominant source of the quadrature error. Gyroscopes have been designed with intentional spring imbalances and fabricated with a SOI-based silicon-on-glass fabrication process, the resulting quadrature outputs of the fabricated gyroscopes have been measured, and their agreement with FEM simulations has been verified. Next, it has been experimentally shown that the electrostatic nulling of the quadrature error with closed-loop control electronics improves the bias instability and angle random walk (ARW) of a fully decoupled gyroscope up to ten times. Moreover, the quadrature cancellation improves the scale-factor turn-on repeatability about four times and linearity about 20 times, reaching down to 119 and 86 ppm, respectively. Finally, the quadrature cancellation allows operating the gyroscope with higher drive-mode displacement amplitudes for an increased rate sensitivity. With this technique, outstanding bias instability and ARW performances of 0.39°/h and 0.014°/$\sqrt{\text{h}}$, respectively, have been achieved. [2011-0078]**

***Index Terms*—Microelectromechanical systems (MEMS) gyro, quadrature-error cancellation, silicon-on-glass (SOG) process, sources of quadrature error.**

I. Introduction

TODAY's gyroscope performance came to a limit that error sources that were not taken into account previously should be considered seriously. Still, there are no microelectromechanical systems (MEMS) gyroscopes satisfying inertial-grade requirements [1], but the trend in reported gyroscopes shows that inertial-grade gyroscopes will exist in the near future. In the path to subdegree-per-hour MEMS gyroscopes, error sources should be well identified, one of the most important being the quadrature motion [2]. The quadrature-error motion is defined as the direct coupling of the drive-mode displacement to the sense mode of the gyroscope and leads to nondiagonal terms in the spring matrix of the gyroscope dynamics [3]. The sources of this error could not be easily identified and controlled, but process imperfections are recognized as the main cause of the quadrature error [4]. Generally, the drive and sense modes of a tuning-fork gyroscope are designed to be perfectly orthogonal to each other. However, typical microfabrication tolerances are poor compared to the dimensions to be fabricated [4], and at the end of the process, inevitable imperfections occur on the orthogonality of the drive and sense modes, resulting in a quadrature error. The quadrature signal is proportional to the drive-mode displacement, and it is different from the angular-rate (Coriolis) signal, which is proportional to the drive-mode velocity. In other words, the phase difference between the angular-rate signal and the unwanted quadrature signal is 90°, suggesting that the quadrature error can be rejected by using a phase-sensitive demodulation. However, even very small phase errors still result in intolerable offset variations at the output of a gyroscope, since the magnitude of the quadrature signal can be as large as a few thousand degrees per second [5], while the angular-rate resolution is desired to be in the order of a few degrees per hour or even less. Therefore, the phase-sensitive demodulation is not a self-sufficient solution in the existence of high quadrature signals.

Since the current microfabrication technologies do not enable fabricating gyroscopes with perfectly orthogonal drive and sense modes, the quadrature error is inevitable, and different approaches have been proposed for its compensation. The earlier approaches used laser trimming the movable mass [6], similar to the method used for tuning the conventional mechanical gyroscopes; however, this is a time-consuming and expensive approach. Another approach is to suppress the quadrature error by careful mechanical design, such as using specially designed mechanical levers [7]–[9]. This approach does not require any additional electronics for quadrature suppression, eliminating the need for a complex readout circuit, as being its main advantage. This method minimizes the quadrature signal, but it cannot remove it completely, i.e., there still remains a residual error signal limiting the performance to values of about 50°/h [7]. A different approach proposes electronic cancellation of the quadrature error by injecting an electronic signal to the input

Manuscript received March 15, 2011; revised December 18, 2011; accepted January 19, 2012. Date of publication April 3, 2012; date of current version May 28, 2012. This work was supported in part by the The State Planning Organization (DPT) of Turkey. Subject Editor F. Ayazi.

E. Tatar and S. E. Alper are with the Micro-Electro-Mechanical Systems Research and Applications Center, Middle East Technical University, Ankara 06531, Turkey (e-mail: erdinctatar@gmail.com; said@metu.edu.tr).

T. Akin is with the Micro-Electro-Mechanical Systems Research and Applications Center, Middle East Technical University, Ankara 06531, Turkey, and also with the Department of Electrical and Electronics Engineering, Middle East Technical University, Ankara 06531, Turkey (e-mail: tayfunakin@metu.edu.tr).

Color versions of one or more of the figures in this paper are available online at http://ieeexplore.ieee.org.

Digital Object Identifier 10.1109/JMEMS.2012.2189356

of the sense-mode preamplifier, the amplitude and phase of which are identical and opposite, respectively, compared to the quadrature signal [10]. It is applicable to any sensor since no mechanical modification is required in the gyro design, but this technique requires a very tight control of both the amplitude and the phase of the feedback signal, which is not easily achievable [6]. A better approach that can eliminate the overall quadrature error by applying differential dc potentials to the mechanical electrodes on the sensor is the electrostatic quadrature cancellation [11]. This approach provides an electromechanical cancellation since it applies electronic feedback signals to the mechanical electrodes which are specifically designed for the quadrature cancellation. These electrodes are capable of generating electrostatic forces inherently inphase with the drive motion, provided that they are biased to differential dc potentials whose amplitude is determined by the electronic feedback circuit. The complete cancellation of the quadrature motion with simple electronics makes this method superior over the other techniques and therefore finds use in the literature's highest performance MEMS gyroscopes [12], [13].

There are also several studies [12]–[14] on the possible sources and cancellation methods of the quadrature error. We have recently reported on the experimental investigation of the quadrature sources and the improvement of the gyroscope performance with the cancellation of the quadrature error [15]. This paper provides additional experimental data over [15] on the sources of quadrature error with the detailed finite element method (FEM) simulations. Simulations include the mass, electrostatic-force, and spring imbalances resulting from typical microfabrication process tolerances. Simulation results indicate that the imbalances in the mechanical springs are the dominant mechanical-error source for the quadrature motion, and these results are verified and consistent with measurement results. This paper also presents improvements in the key performance parameters of gyroscopes, such as bias instability, angle random walk (ARW), and zero-rate offset with the cancellation of the quadrature error. In addition to [15], this study reports the experimental results showing the effects of quadrature cancellation on the gyroscope parameters such as bias repeatability, scale-factor repeatability, and linearity, which are also critical parameters for tactical- and inertial-grade gyroscopes. Finally, it has been observed that the quadrature cancellation enables higher drive-mode displacement amplitudes for a low-noise operation without suffering from a high zero-rate output offset. This technique is applied to one of the gyroscopes fabricated in this work, where this gyroscope achieves bias instability and ARW performances exceeding the tactical-grade requirements.

II. Analyses on the Sources of the Quadrature Error

It is difficult to find the exact sources of the quadrature error, but the known fact is its occurrence due to the direct coupling of the drive-mode displacement into the sense mode. The major sources of the quadrature error include any imbalance in the mechanical springs, electrostatic force, and vibrating mass [6]. Observation of the results of probable process imperfections on the quadrature error is one of the main objectives of this study, along with its cancellation. Gyroscopes with intentional imperfections are designed, simulated, and fabricated in this work in order to identify the dominant source contributing to the quadrature error.

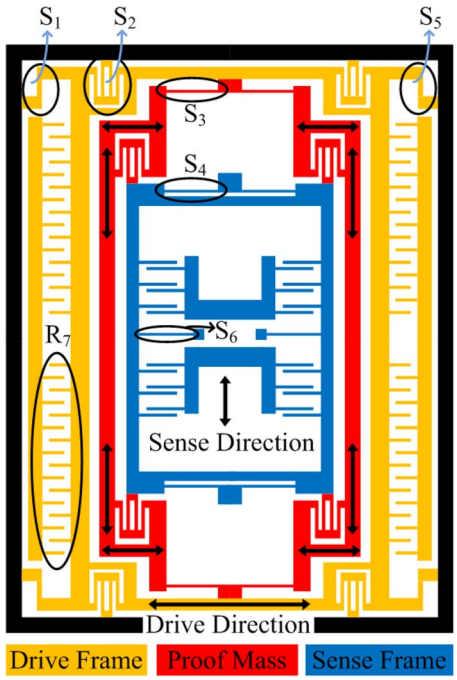

Fig. 1. Conceptual half view of the gyroscope used in this study.

The device layer of the gyroscope fabricated in this work requires a single dry-etch step (DRIE). Any imperfection due to a lithography or etch tolerance may result in a quadrature error. The effects of less serious imperfections such as the mass and electrostatic-force imbalances are analyzed in Section II-A, which is followed by a separate section (Section II-B) analyzing the more serious imperfection, which is the spring imbalance. It should be mentioned that the electrical feedthrough coupling is not analyzed in this study as a quadrature source as the gyroscope in this study is operated under the mismatch conditions with a capacitive preamplifier interface, i.e., any coupling from the drive to sense signal affects the inphase rate signal instead of the out-of-phase quadrature signal.

A. *Effect of the Mass and Electrostatic-Force Imbalances on the Quadrature Error*

Fig. 1 shows the conceptual half view of the gyroscope used in this study; the numbered springs (S_1–S_6) and region (R_7) are examined in terms of their contribution to the quadrature error. The gyroscope consists of three separate and movable frames, which are the drive, proof mass, and sense frames. The drive and sense frames have a 1-degree-of-freedom (DOF) motion capability, while the proof mass, which is responsible to establish the Coriolis coupling between the drive and sense frames, has a 2-DOF motion capability. The drive and proof-mass frames move along the drive-mode direction in Fig. 1, and if the substrate is subject to a rotation along the out-of-plane axis, the proof-mass and sense frames start moving along

TABLE I
SIMULATED QUADRATURE-ERROR RESULTS FOR THE MASS AND ELECTROSTATIC-FORCE IMBALANCES, SHOWING THAT THE FORCE IMBALANCES RESULT IN HIGHER QUADRATURE ERRORS

Quadrature source	Nominal value	Errored value	Quadrature error (°/s)	Sense/drive coupling (ppm)
Mass imbalance	0	1/80	10	17.4
Force imbalance Gap of R_7	2μm	2.2μm	92.7	161.2
		2.5μm	178	309.7

the sense-mode direction, which is ideally orthogonal to the drive-mode direction. Theoretically, the drive and sense modes are completely decoupled from each other by the mechanical design, but they could not be fabricated exactly orthogonal to each other due to the process imperfections, which results in a quadrature-error motion. Complete decoupling refers to satisfying the following two conditions: 1) The sense mode should remain stationary during drive-mode vibrations provided that there is no applied angular rate, and 2) any vibration arising along the sense mode due to an angular-rate input does not affect the drive-mode vibrations either.

In order to observe the effect of mass imbalance on the quadrature error, the bottom half portion of the movable drive fingers in the R_7 region shown in Fig. 1 has been deleted during the FEM simulations, which are conducted by the CoventorWare software. The validity of FEM simulations is verified after a convergence study in which simulations were run by decreasing the mesh size by $\sqrt{2}$ until reaching an error rate of 1%. Simulated mass imbalances are 1/500, 1/200, and 1/80, where these fractions show the ratio of the amount of deleted mass to the total movable mass in the drive mode. Simulation results show that quadrature errors are lower than $10^\circ/\mathrm{s}$ even with the exaggerated mass-imbalance condition of 1/80, i.e., it can be concluded that the mass imbalance does not cause a significant quadrature error for the given decoupled gyroscope structure. The next analyzed imbalance is the electrostatic-force imbalance, which arises from the drive fingers that do not have an identical capacitive gap spacing due to the process imperfections. Table I summarizes the results of the simulated quadrature errors for the mass and electrostatic-force imbalances. The nominal 2-μm capacitive gaps of the drive fingers are modified in the region R_7 in Fig. 1 to 2.2 and 2.5 μm in the FEM simulations, which yield quadrature errors of $93^\circ/\mathrm{s}$ and $178^\circ/\mathrm{s}$, respectively. It is clear that the force imbalance results in higher quadrature errors compared to the mass imbalance, considering typical process variations. The final source of the quadrature error analyzed in this work is the effect of spring imbalances, which is discussed separately in the next section.

B. Effect of the Spring Imbalances on the Quadrature Error

The final and most important quadrature-error source analyzed in this study is the spring imperfections. First of all, the effect of an intentional misalignment has been examined. If spring S_3 in Fig. 1 is misaligned by 1° from the drive-mode direction, then the resulting quadrature error is simulated to be $1800^\circ/\mathrm{s}$ which corresponds to a drive-to-sense coupling of 3132 ppm. The amount of the simulated error is quite high, but a 1° misaligned spring is also an exaggerated case and cannot occur with a typical process tolerance. A second and more probable fact that can cause spring imbalance is the variation of spring widths during the fabrication process. In the same device, the widths of the springs may be different after the fabrication due to the variations in the uniformity of both the lithography and etch steps, even though they have identical dimensions in the layout. The nominal width of all the springs in the gyroscope used in this work is designed as 4 μm. The effects of different spring imbalances have been simulated, each time changing the width of only one spring among springs S_1–S_6 in Fig. 1. Table II shows the simulated quadrature-error results for different spring imbalances caused by the spring-width variations.

TABLE II
SIMULATED QUADRATURE-ERROR RESULTS FOR DIFFERENT SPRING IMBALANCES CAUSED BY SPRING-WIDTH VARIATIONS; CLEARLY, S_3 CAUSES A HIGHER QUADRATURE ERROR

Imbalanced Spring	S_1	S_2	S_3	S_4	S_5	S_6
Modified Width (μm)	3.5	3.5	3.6/3.8	3.5/3.8	3.5	3.5
Resulting Quadrature (°/s)	30	13.2	438/228	9.7/4	43.4	0.1
Sense/drive Coupling (ppm)	52.2	22.9	762/396	17/7	75.5	0.17

By observing Table II, the highest quadrature error is introduced by the imperfection in spring S_3. Different from the other springs, spring S_3 transmits the drive force from the drive frame to the proof-mass and sense frames. The quadrature error occurs due to the coupling of drive displacement into the sense mode, and an imperfection in the force-transmitting springs is expected to cause a higher quadrature error compared to the others. Spring S_5, which connects the drive frames of differential gyroscopes, also causes a relatively higher quadrature error, but this appears as a common-mode error for the tuning-fork gyroscopes, which can be eliminated by differential reading. Springs S_4 and S_6 are similar to spring S_3 in terms of their geometrical structure, but they do not cause that much quadrature error, since they do not transmit the drive force, which also explains the small quadrature errors simulated for springs S_1 and S_2. Depending on the simulation results summarized in Tables I and II, the imperfection in spring S_3 is selected for experimental evaluation, since it has been simulated as the dominant source of the quadrature error considering typical imbalances. The intentional imperfection on spring S_3 is introduced by using two different spring widths in the fabrication mask layout, as 3.6 and 3.8 μm, whereas the nominal value of the remaining springs of the gyroscope is kept as 4 μm. In addition, the mask layout also includes gyroscopes that do not contain any intentional imperfection. These ideal gyroscope layouts are located in close neighborhood of the gyroscopes that have intentional imperfections. This approach helps making meaningful comparisons between the two designs, as both would be subject to similar unintentional process variations.

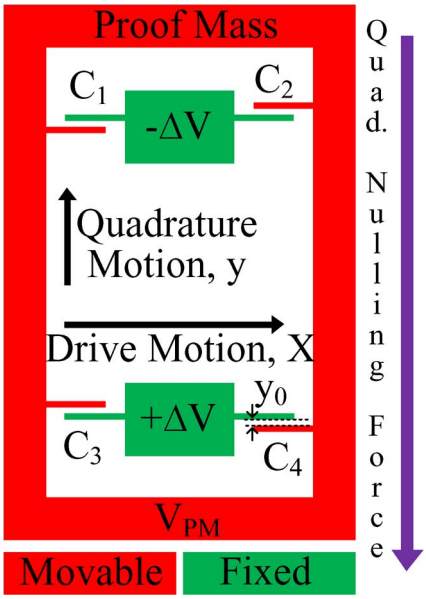

Fig. 2. Conceptual quadrature-error-cancellation configuration. The phase condition of the quadrature force is satisfied by the comb finger capacitances (C_1–C_4).

III. Electrostatic Quadrature Cancellation

A. Design of the Quadrature Cancellation Electrodes

The complete suppression of the quadrature motion requires a force, exactly inphase with the drive displacement, applied to the sense mode. Fig. 2 conceptually shows this quadrature-error-cancellation configuration, which satisfies the phase consistency by a special configuration of the comb finger capacitances ($C_1, C_2, C_3,$ and C_4) [11] and is also adapted to the gyroscope fabricated in this study.

For the drive motion direction in Fig. 2, the provided capacitance configuration generates an electrostatic quadrature cancellation force when there is a nonzero quadrature motion (y), which is detected by the closed-loop quadrature cancellation electronics. This electronics generates the proper quadrature nulling dc potentials $\pm\Delta V$ that are applied to the capacitance configuration in Fig. 2. The resulting quadrature cancellation force is expressed as

$$F_Q = -\frac{4 \cdot V_{\mathrm{PM}} \cdot \Delta V \cdot \varepsilon \cdot X \cdot h}{y_0^2} \tag{1}$$

where V_{PM} is the proof-mass potential, ε is the permittivity of the free space, X is the drive displacement, h is the structural thickness, and y_0 is the capacitive gap for the nulling electrodes.

Equation (1) is valid for $y \ll y_0$, which is typically the case. The negative sign in (1) indicates that the capacitance–voltage configuration in Fig. 2 acts to stop the unwanted quadrature motion. The force expression in (1) includes the sinusoidal drive displacement X, which inherently guarantees a zero phase error between "the force causing quadrature motion" and "the quadrature nulling force." The quadrature error can then be easily cancelled by applying only $\pm\Delta V$ dc potentials to the quadrature cancellation electrodes.

Fig. 3 shows the conceptual half view and SEM image of the fully decoupled gyroscope developed at Middle East Technical University (METU) including the quadrature cancellation electrodes, which are placed on the proof-mass frame. With this way, the electrodes make use of the drive displacement to modulate the quadrature cancellation force and exert this force on the sense-mode dynamics to stop the unwanted quadrature motion. The sense-mode dynamics can be modeled as a second-order spring-mass-damper system, and the relation between the existing quadrature displacement (Y_Q) and the corresponding nulling force (F_Q) can be written as

$$\frac{Y_Q(s)}{F_Q(s)} = \frac{1}{m_S\left(s^2 + \frac{w_S}{Q_S}s + w_S^2\right)} \tag{2}$$

where m_S is the mass of the sense mode, w_S is the sense-mode resonance frequency, and Q_S is the quality factor of the sense mode. Noting that the gyroscope is operated at the drive-mode resonance frequency ($s = jw_D$) and under vacuum conditions (therefore, Q_S is a few thousands or more), the imaginary part of (2) can be neglected as follows:

$$\frac{Y_Q(s)}{F_Q(s)} = \frac{1}{m_S\left(w_S^2 - w_D^2\right)} = \frac{1}{\underbrace{k_S - m_S w_D^2}_{k_{\mathrm{effective}}}} \tag{3}$$

where k_S is the mechanical-spring constant of the sense mode. Equation (3) provides the well-known force-displacement characteristics of an ideal spring ($F = kY$) under static conditions ($w_D = 0$). However, at dynamic conditions, the second term in the denominator of (3) decreases the effective spring constant of the sense mode and increases the maximum amount of the quadrature-error motion that can be cancelled for a fixed quadrature cancellation force F_Q. Substituting (1) into (3) and rearranging the terms result in

$$\frac{4 \cdot V_{\mathrm{PM}} \cdot \Delta V \cdot \varepsilon \cdot X \cdot h}{y_0^2} = Y_Q \cdot k_{\mathrm{effective}} \tag{4}$$

where $k_{\mathrm{effective}}$ is the effective spring constant of the sense mode found by (3). ΔV in (4) determines the maximum amount of the quadrature motion that can be cancelled with the given configuration. The maximum ΔV is limited by the closed-loop feedback control electronics.

B. Design of Control Electronics for the Quadrature-Error Cancellation

Fig. 4 shows the block diagram of the quadrature control electronics. The output of the gyroscope sense mode (SP) is first demodulated with a 90° phase-shifted version of the drive-pick (DP) signal, and the resulting rectified signal is passed through a low-pass filter (LPF) to get the amplitude information of the quadrature signal. Then, the quadrature amplitude is compared to null, and the error output is fed to a PI controller. The PI controller generates the dc potential ΔV which is differentially applied to the quadrature electrodes (Q+ and Q−). The structure of the quadrature cancellation electrodes inherently modulates these dc potentials to the drive-mode frequency, generating the proper quadrature cancellation force exactly inphase with the drive displacement.

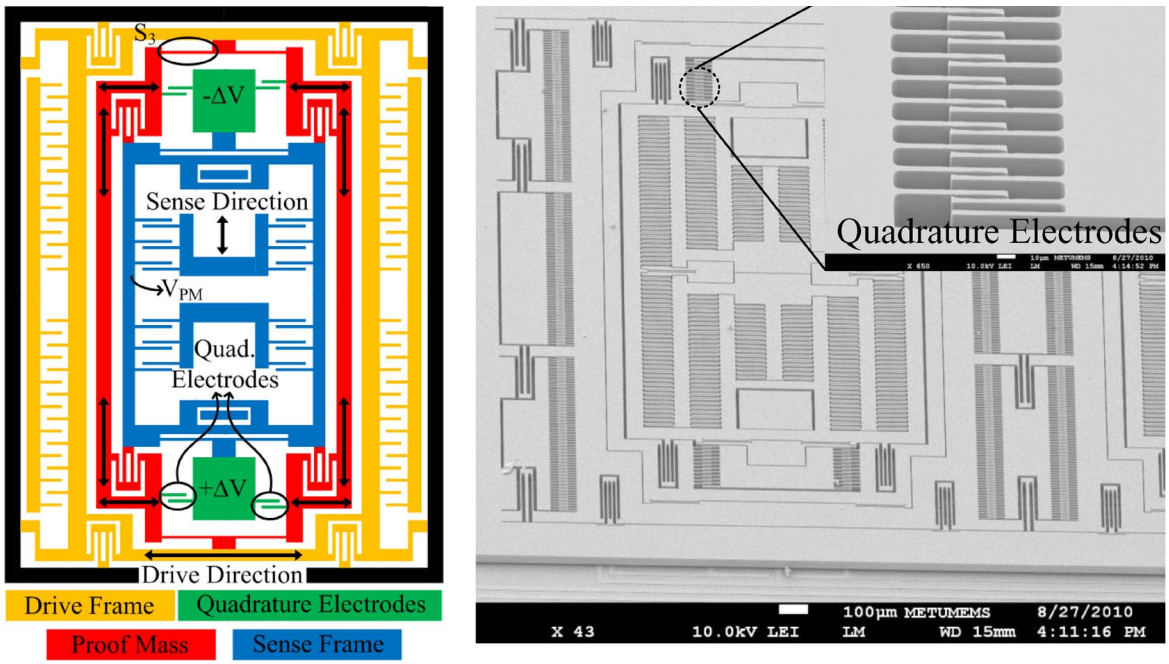

Fig. 3. (Left) Conceptual half view and (right) SEM image of the fully decoupled gyroscope developed at METU, including the quadrature cancellation electrodes, which are placed on the proof-mass frame. The electrodes make use of the drive displacement to modulate the quadrature cancellation force and exert the force on the sense-mode dynamics. The SEM image is the view of the SOI wafer from the bottom after bonding to glass and removing the SOI handle.

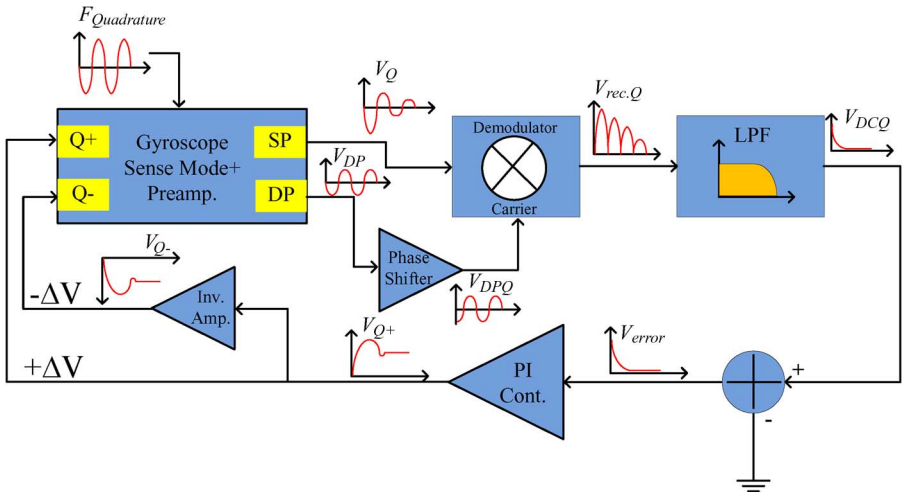

Fig. 4. Block diagram of the quadrature control electronics.

No bandwidth considerations exist for the given quadrature circuit since the frequency of the quadrature signal is always constant at the drive-mode resonance frequency (do not change when a time-varying rate is applied). This property greatly simplifies the controller design for the system. The second-order sense-mode dynamics of the gyroscope can be modeled as a constant gain stage running exactly at the drive-mode resonance frequency, and an open-loop transfer function of this system can then be expressed as

$$H_{\mathrm{OL}}(s) = \frac{V_Q(jw_D)}{F_Q(jw_D)} \cdot K_D \cdot H_{\mathrm{LPF}}(s) \cdot H_{\mathrm{PI}}(s) \cdot K_{\mathrm{quad}}. \quad (5)$$

In (5), V_Q is the voltage observed at the SP output due to the motion resulting from a quadrature force F_Q, K_D is the gain of demodulator, $H_{\mathrm{LPF}}(s)$ is the transfer function of LPF, $H_{\mathrm{PI}}(s)$ is the transfer function of the PI controller, and K_{quad} is the gain of mechanical-quadrature-cancellation configuration and can be extracted from (1) as

$$K_{\mathrm{quad}} = \frac{F_Q}{\Delta V} = \frac{4 \cdot V_{\mathrm{PM}} \cdot \varepsilon \cdot X \cdot h}{y_0^2}. \quad (6)$$

Equation (5) is used to obtain the parameters of the PI controller. Note that the open-loop transfer function is dominated by the LPF and PI controller characteristics. The zero introduced by the PI should be far away from the poles of LPF so that the system operates as expected, which can be achieved by setting the proportional gain to zero and by using only the integral gain.

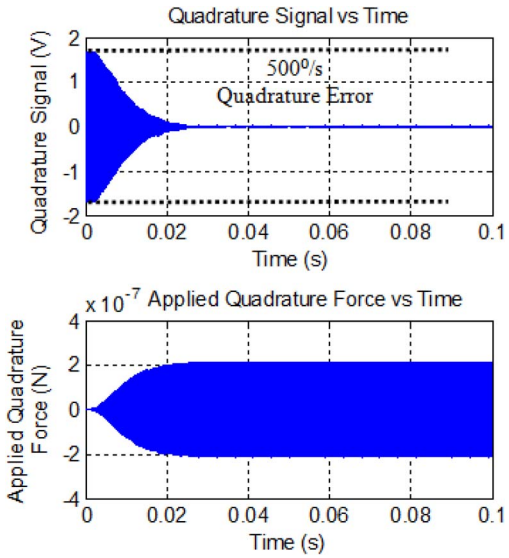

Fig. 5. Simulated response of the system to a 500°/s quadrature signal, where the upper figure shows the decrease of the quadrature signal over time while the lower figure shows the increase in the applied quadrature force over time. The settle time is 30 ms.

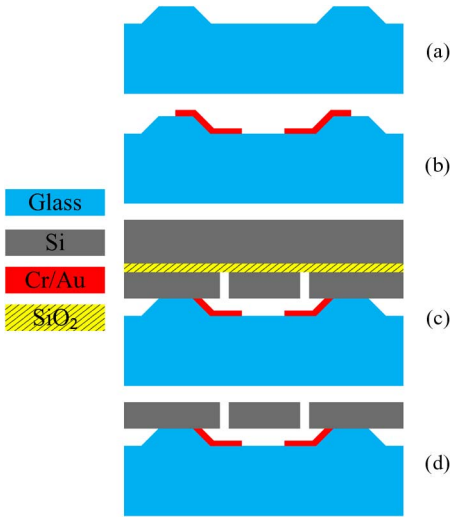

Fig. 6. Process flow of the SOI-wafer-based SOG micromachining process.

The behavioral model of the system in Fig. 4 is constructed in the SIMULINK design environment. Fig. 5 shows the response of the system to a typical 500°/s quadrature signal, where the upper figure shows the decrease of the quadrature signal over time while the lower figure shows the increase in the applied quadrature force over time. The unwanted quadrature signal is canceled, and the system reaches to steady state within 30 ms.

IV. Fabrication

The gyroscopes are fabricated with an in-house silicon-on-insulator (SOI)-wafer-based silicon-on-glass (SOG) micromachining process, where a simplified flow of the fabrication is shown in Fig. 6. The process starts with the preparation of a glass wafer by forming the anchors (a) and then the interconnect metallization (b). Next, the device layer is patterned on a SOI wafer using DRIE, for which the buried oxide of the SOI wafer is used as an etch stop layer. Then, the patterned SOI and glass wafers are anodically bonded to each other by a process similar to standard silicon–glass anodic bonding, without directly applying a bias to the patterned device layer of SOI wafer (c). The process ends with the releasing of the structures by dissolving the handle layer and buried oxide of the SOI wafer (d). The image on the right in Fig. 3 shows the SEM image of one of the fabricated gyroscopes together with a close-up view of the quadrature cancellation electrodes. The SEM image is the view of the SOI wafer from the bottom after bonding to glass and removing the SOI handle.

Performing DRIE on a SOI wafer rather than on a recessed glass wafer has a significant advantage of having more stable process conditions over the classical SOG process [16]. Performing DRIE on a recessed glass wafer in the classical SOG process has reliability problems, and the ways to overcome this problem are reported in [17]. The capacitive drive gaps are widened in the SOG process to 2.5 μm; however, it is reduced to 2.18 μm in the current process, both having a design value of 2 μm. Table III shows the designed and measured values of the gyroscope parameters.

TABLE III
Designed and Measured Values of the Gyroscope Parameters

Parameter	Design Value (μm)	Measured Value (μm)
Capacitive drive gap	2	2.18
Capacitive sense gap	2	2.43
Capacitive sense antigap	7	7.30

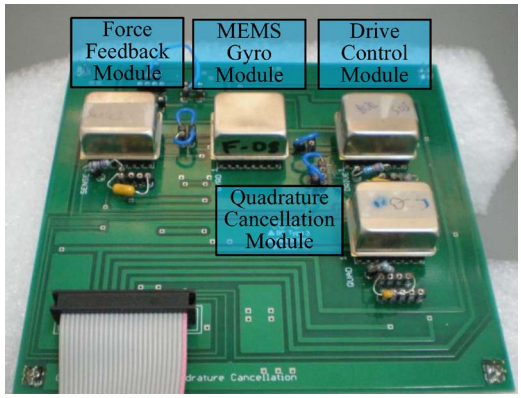

Fig. 7. Test PCB containing the complete gyroscope system. The modules are integrated in hybrid packages for low-noise measurements.

V. Test Results

The fabricated gyroscopes with and without intentional imperfections have been integrated with the closed-loop control electronics on a printed circuit board (PCB). Fig. 7 shows the PCB containing the complete gyroscope system under test, in which the gyroscope module and closed-loop electronic modules are integrated in hybrid packages for low-noise measurements. The complete gyroscope system consists of four separate modules: *MEMS Gyro Module* contains the sensor element and preamplifiers, *Drive Control Module* locks on the drive-mode resonance frequency and sets the amplitude of

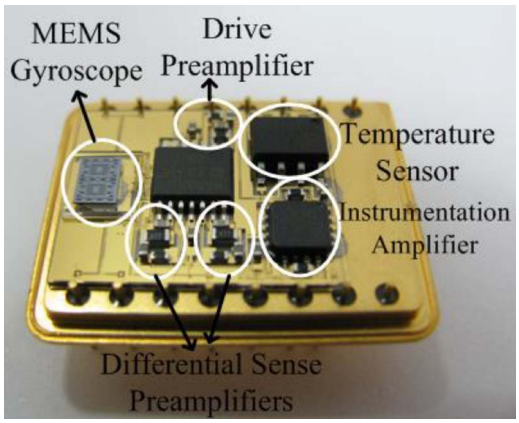

Fig. 8. *MEMS Gyro Module* showing the MEMS gyroscope and preamplifiers.

TABLE IV
COMPARISON OF THE SIMULATED AND MEASURED RESULTS FOR THE DIFFERENT WIDTHS OF THE INTENTIONALLY MODIFIED SPRING S_3. THE RESULTS AGREE WITH EACH OTHER, AND THE MISMATCH IS DUE TO THE UNAVOIDABLE PROCESS TOLERANCES

Width of S_3 (Fig. 1)	Quadrature Error (°/s)			
	Simulated		Measured	
3.6μm	438°/s	762ppm	450°/s	782ppm
3.8μm	228°/s	396ppm	391°/s	680ppm
4μm	0	0	75°/s	130ppm

drive displacement, *Force-Feedback Module* controls the sense mode and generates the rate output, and finally, *Quadrature-Cancellation Module* suppresses the quadrature motion. *MEMS Gyro Module* is vacuum packaged to reduce the Brownian noise floor of the gyroscope. All of these modules are implemented with discrete components, and Fig. 8 shows the inside of a sample *MEMS Gyro Module* containing the MEMS gyroscope and preamplifiers.

A. Test Results on the Sources of the Quadrature Error

Gyroscopes with intentionally placed spring imperfections are fabricated and tested. Table IV provides the comparison of the simulated and measured results for the different widths of the intentionally modified spring S_3, which are in agreement. The mismatch between the simulated and measured results is due to the unavoidable process tolerances, i.e., there is already an amount of quadrature error in the perfectly drawn gyros. In the actual gyroscope, there exist eight springs which are same as spring S_3, but only one of them is simulated. We cannot guarantee that all of the springs will be in the same width after fabrication; even a 0.1-μm width difference may result in a $75^\circ/\text{s}$ quadrature error. The simulation and measurement results in Table IV also show that even a small variation in the width of the springs may cause high quadrature errors, as predicted from the simulations.

Table V shows the measured and designed spring widths of the ideal and modified gyroscopes. The width of the modified springs is thinner by almost 200–400 nm than the ideal spring which is consistent with the design. The deviation from the designed values is due to unavoidable process tolerances.

TABLE V
MEASURED AND DESIGNED SPRING WIDTHS OF THE IDEAL AND MODIFIED GYROSCOPES. THE EFFECT OF INTENTIONAL MODIFICATION CAN BE SEEN

Designed Width of S_3 (Fig.1)	Measured Width of S_3 by SEM
4μm	3.51μm
3.8μm	3.33μm
3.6μm	3.21μm

TABLE VI
OPERATION PARAMETERS OF ONE OF THE TESTED GYROSCOPES

Gyroscope Parameter	Value
Drive Mode Resonance Frequency (f_{drive})	12.72kHz
Drive Mode Quality Factor (Q_{drive})	48586
Proof Mass Potential (V_{PM})	13V
Sense Mode Resonance Frequency (f_{sense})	12.59kHz
Sense Mode Quality Factor (Q_{sense})	2518
Drive Displacement Amplitude (X_{drive})	3.5μm
Frequency Mismatch ($\Delta f = f_{drive} - f_{sense}$)	130Hz
Sense mode capacitance (C_{sense})	10.3pF
Sense mode capacitance gradient ($\partial C_{sense}/\partial y$)	2.7μF/m
Pressure level inside the cavity	~200 mTorr

B. Gyroscope Performance With and Without the Quadrature Cancellation

The gyroscope studied in this work is a tuning-fork type having two separate sense masses. The quadrature level of each tine is different due to process variations, and the outputs of the two tines are picked up differentially. If the quadrature motions of the differential tines are also in the opposite direction, they would be added and cancelled by the quadrature control loop. In case their amplitudes are not identical, the quadrature nulling signal would cause a residual motion of the tines, but this residual motion would cause both tines to move in the same direction. Such a motion is inherently rejected by the differential reading. The separate cancellation of the quadrature of each tine is also possible, and that kind of an approach would result in exact cancellation. However, this approach would double the gyroscope layout and circuit complexity; therefore, it is not preferred in this study.

Table VI summarizes the operation parameters of one of the tested gyroscopes. We operated the gyroscopes under mismatch conditions with a drive–sense resonance-frequency difference of 100–150 Hz. The dc quadrature cancellation potentials also affect the sense–drive frequency mismatch, and it is included in the measurements.

The quality factor of the sense mode is significantly lower than that of the drive mode because the dominant damping mechanism in the varying gap-type sense fingers is the squeeze film damping which results in a higher damping coefficient compared to the slide film damping in the varying overlap type drive fingers. In addition, the unbalanced torque created by the differential movement of the sense tines on the substrate also reduces the sense-mode quality factor.

The constructed quadrature cancellation circuit is tested and verified to null the quadrature signals up to $\pm 730^\circ/\text{s}$ with dc nulling potentials less than ± 2.5 V, contrary to the high (up to 20 V) cancellation voltages reported in [12] and [13]. Increasing the supply potentials of the controller circuit will

TABLE VII
SCALE-FACTOR TEST RESULTS WITH AND WITHOUT QUADRATURE CANCELLATION, SHOWING A SLIGHT INCREASE WITH THE QUADRATURE CANCELLATION DUE TO THE REDUCED PHASE ERRORS IN THE ELECTRONICS

Gyro ID	Scale Factor, mV/(°/s)	
	With Quadrature Cancellation	Without Quadrature Cancellation
#1	7.46	7.29
#2	7.54	7.50
#3	7.05	6.9

TABLE VIII
EXPERIMENTAL DEMONSTRATION OF THE PERFORMANCE IMPROVEMENT WITH THE QUADRATURE-ERROR CANCELLATION FOR A 3.5-μm DRIVE DISPLACEMENT, VERIFYING THE IMPROVEMENTS IN THE ARW AND BIAS INSTABILITY BY AN ORDER OF MAGNITUDE

Performance Parameters		Gyro#1	Gyro #2
Zero Rate Output (mV)	WITH Quad. Cancellation	0.25	2.5
	WITHOUT Quad. Cancellation	-207	223
	Factor of Improvement	**828**	**89.2**
Bias Instability (°/hr)	WITH Quad. Cancellation	0.91	3.1
	WITHOUT Quad. Cancellation	7.1	12
	Factor of Improvement	**7.8**	**3.9**
ARW (°/√hr)	WITH Quad. Cancellation	0.034	0.07
	WITHOUT Quad. Cancellation	0.36	0.49
	Factor of Improvement	**10.6**	**7**
Quadrature Error Before Cancellation (°/s)		450	500
Quadrature Error Before Cancellation (ppm)		782	870

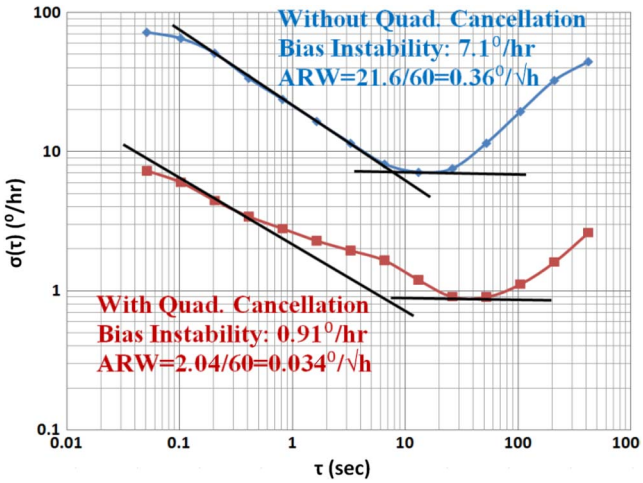

Fig. 9. Allan variance graphs of Gyro#1 with and without the quadrature cancellation, presenting the improvement with the quadrature cancellation by factors up to 10.

TABLE IX
ZRO AND ARW RELATION OF DIFFERENT GYROSCOPES WITHOUT THE QUADRATURE CANCELLATION. GYROSCOPES WITH LOWER ZRO (QUADRATURE SIGNAL) HAVE A BETTER ARW PERFORMANCE

Gyro ID	ZRO (mV)	ARW (°/√hr)
#1	-207	0.36
#2	223	0.49
#3	-12.5	0.037

directly improve the maximum quadrature error that can be cancelled.

Ideally, the quadrature cancellation circuit should only cancel the quadrature signal and should not deteriorate the Coriolis (rate) signal. This is verified by the scale-factor tests, and Table VII presents the scale-factor measurements. The measurements are obtained under the identical test conditions for the quadrature cancellation circuit for two cases: active (i.e., with the quadrature cancellation) and inactive (i.e., without the quadrature cancellation). Scale factors with quadrature cancellation are observed to be slightly higher and close to the design value. This is due to the fact that the phase-sensitive demodulation in the force-feedback electronics becomes more accurate with the quadrature nulling since the quadrature signal and phase error act in a way to decrease the scale factor. This is the result of a phase-sensitive demodulation of one inphase and one 90°-phase signals in the presence of a phase error.

Table VIII provides the test results showing the effect of the quadrature cancellation on the gyro performance for a drive-displacement amplitude of 3.5 μm. If the inherent quadrature signal in the gyroscope output is not canceled, it causes a high zero rate output (ZRO) due to the phase errors in the force-feedback electronics. ZRO decreases by two to three orders of magnitude with nulling the quadrature signal. In addition, the bias instability and ARW performances of the gyroscopes are improved by factors up to eight and ten, respectively, with the quadrature cancellation. Fig. 9 shows the Allan variance graphs of Gyro#1 for a 3.5-μm drive displacement both with and without the quadrature cancellation, presenting the improvement with the quadrature cancellation. This is a result of keeping the sense mode free of unwanted vibrations due to the quadrature motion, which disturbs the angular-rate response. These results also indicate that the unwanted quadrature motion introduces extra noise to the system. We believe that this is due to the uncertainty on the quadrature signal, which feeds to the angular-rate output with a certain coupling coefficient depending on the phase errors in the system (ideally, no quadrature signal passes to the output due to phase-sensitive demodulation). The uncertainty may originate from the noise in the quadrature signal or the drift of the quadrature signal. These mean that the smaller the amplitude of the quadrature signal, the smaller the uncertainty that couples to the angular-rate output. In addition, Table IX shows the correlation between the amplitude of the quadrature signal and the ARW performances. We compared the ARW of the gyroscopes without the quadrature cancellation. Gyroscopes with a lower ZRO (quadrature error) have a better ARW performance; in other words, the lower the quadrature, the better the performance.

The turn-on repeatability of the scale factor and bias are important performance parameters for tactical- and navigation-grade gyroscopes. The repeatability tests have been performed according to the procedure described in IEEE Standard 952-1997 by powering up the sensor, waiting for the heat-up period, measuring the scale factor, turning off the power, waiting for cooling down, and repeating this cycle for five times. Both of these parameters are experimentally evaluated on the fabricated gyroscopes with and without the quadrature cancellation. Table X presents the scale-factor repeatability-test results of Gyro#1 with and without the quadrature cancellation, showing that the quadrature cancellation improves the scale-factor repeatability by a factor of almost four as a result of more effective and stable phase-sensitive demodulation.

TABLE X
SCALE-FACTOR TURN-ON REPEATABILITY-TEST RESULTS OF GYRO#1 WITH AND WITHOUT THE QUADRATURE CANCELLATION. THE QUADRATURE CANCELLATION IMPROVES THE SCALE-FACTOR REPEATABILITY BY A FACTOR OF ALMOST FOUR

Test	Scale factor w/o quadrature canc. (mV/^{0}/s)	Scale factor with quadrature canc. (mV/^{0}/s)
#1	7.29077	7.46343
#2	7.28814	7.46144
#3	7.28447	7.46189
#4	7.28946	7.4632
#5	7.28209	7.4631
Scale factor repeatability (ppm)	**495 (1σ)**	**119 (1σ)**

TABLE XI
BIAS–TURN-ON-REPEATABILITY TEST RESULTS OF GYRO#1 WITH AND WITHOUT THE QUADRATURE CANCELLATION. A NOTABLE IMPROVEMENT COULD NOT BE OBSERVED POSSIBLY DUE TO THE UNCONTROLLED AMBIENT TEMPERATURE VARIATIONS

Test	Mean of the data w/o quadrature canc. (mV)	Mean of the data with quadrature canc. (mV)
#1	-197.064	1.94
#2	-197.076	1.957
#3	-197.065	1.965
#4	-197.098	1.972
#5	-197.094	1.976
Bias repeatability (^{0}/hr)	**7.87 (1σ)**	**6.88 (1σ)**

Table XI presents the bias-repeatability test results of Gyro#1 with and without the quadrature cancellation, for which there is no significant improvement observed with the quadrature cancellation. However, these tests could not be performed in a controlled temperature environment; therefore, the effects of temperature variation during the tests are believed to be the dominating factor in the bias-repeatability test results.

All the gyroscopes in this work have been verified to have an operating range of $\pm 100^\circ/\mathrm{s}$, provided that the ZRO is close to zero. An increased ZRO reduces the operating range of the gyroscopes without the quadrature cancellation since the rate output is limited by the supply potentials. The operating range is restored with the quadrature nulling, since the quadrature cancellation effectively reduces the ZRO.

The effect of the quadrature cancellation on linearity is also investigated experimentally. Fig. 10 shows the gyro output versus the applied rate for Gyro#1 with and without the quadrature cancellation. The linearity of Gyro#1 in the range $\pm 100^\circ/\mathrm{s}$ is 1982 ppm without the quadrature nulling, while this value improves to 86 ppm with the quadrature nulling. These are consistent with the peak-to-peak noise of Gyro#1 in the full scale range $(\pm 100^\circ/\mathrm{s})$ which is 1980 ppm without the quadrature cancellation and 187 ppm with the quadrature cancellation. Fig. 11 shows the residuals of Fig. 10, i.e., the error between the actual data and the fitted line when the quadrature cancellation is active and not active. The residuals exhibit random characteristics without the quadrature cancellation; however, they have a certain shape with the quadrature cancellation. Although not performed in this study, the linearity

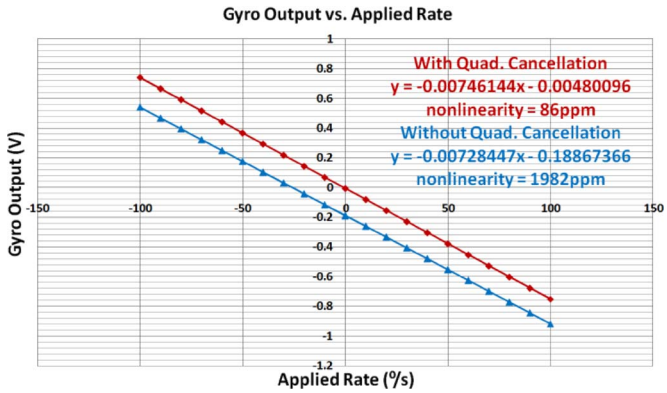

Fig. 10. Gyroscope output versus the applied rate for Gyro#1 with and without the quadrature cancellation. The linearity of the gyroscope improves by a factor of almost 20 with the quadrature cancellation.

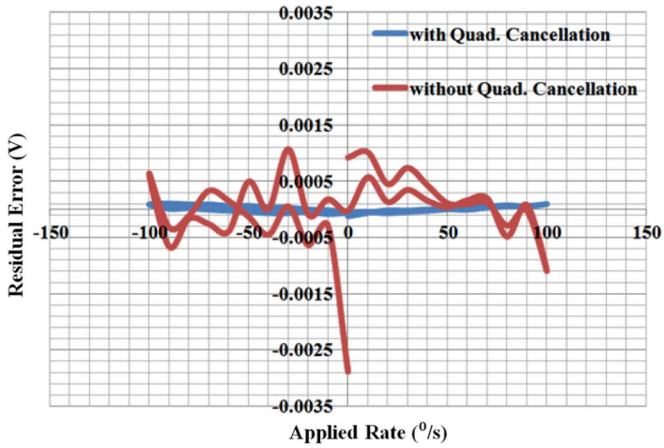

Fig. 11. Residuals of Fig. 10, i.e., the error between the actual data and the fitted line to calculate the linearity of the sensor when the quadrature cancellation is active and not active. The residuals exhibit random characteristics without the quadrature cancellation; however, they have a certain shape with the quadrature cancellation.

of the sensor with the quadrature cancellation can further be improved by characterizing the behavior in Fig. 11. Figs. 10 and 11 show that the linearity improvement with the quadrature cancellation is due to the fact that the quadrature cancellation reduces gyro noise and brings the linearity errors to a systematic nonlinearity level.

The gyroscope bandwidth is not affected by the quadrature cancellation since the bandwidth of the gyroscope is determined by the electronic filter stage in the sense-mode electronics. Although it is not experimentally verified, the bandwidth assumption is valid for the gyroscopes operating in mismatched mode. The quadrature cancellation can only affect the bandwidth in mismatched mode when the frequency shift caused by the quadrature potentials decreases the mismatch to a considerable value. It has been calculated that the spring-softening effect caused by these potentials is less than 1/25 of that generated by the sense-mode fingers which have no major effect in this system.

C. *Increasing the Noise Performance of the Gyroscope*

1) Noise Analysis of the Mechanical Structure and Readout Electronics: Mechanical noise in movable MEMS structures

TABLE XII
PERFORMANCE RESULTS OF THE GYROSCOPES WITH 3.5- AND 7-μm DRIVE DISPLACEMENTS WITH AND WITHOUT THE QUADRATURE CANCELLATION

Performance Parameters		Gyro#1		Gyro #4	
Drive Mode Displacement		3.5µm	7µm	3.5µm	7µm
ZRO (mV)	with Quadrature Canc.	0.25	1.5	-4	-8
	w/o Quadrature Canc.	-207	2500	2500	2500
ARW (^{0}/√hr)	with Quadrature Canc.	0.034	0.015	0.029	0.014
	w/o Quadrature Canc.	0.36	-*	-*	-*

* Could not be measured due to the saturated force-feedback electronics as a result of a high Zero Rate Output (ZRO).

is dominated by the Brownian motion of air molecules. The Brownian force causing this noise motion can be expressed by [18]

$$F_B = \sqrt{4 \cdot k_B \cdot T \cdot b} \tag{7}$$

where k_B is the Boltzmann's constant, T is the ambient temperature, and b is the damping constant. For the gyroscope under evaluation, the noise-equivalent rate can be defined by the ratio of the Brownian force to the Coriolis force as follows:

$$\Omega_{\text{rate}} = \frac{\sqrt{4 \cdot k_B \cdot T \cdot \frac{m_S \cdot w_S}{Q_S}}}{2 \cdot m_{\text{PM}} \cdot w_D \cdot X_D}. \tag{8}$$

The mechanical-noise-equivalent rate is calculated as $1.71^\circ/\text{h}/\sqrt{\text{Hz}}$ using (8) for the gyroscope whose operation parameters are summarized in Table VI (with $m_S = 1.686 * 10^{-7}$ kg and $m_{\text{PM}} = 6.4 * 10^{-8}$ kg). Note that this is the mechanical noise. In the final noise calculation, the noise coming from the electronics should also be included, and it is found to be $0.85^\circ/\text{h}/\sqrt{\text{Hz}}$ for the same gyroscope. The Brownian noise-equivalent rate (Ω_{rate}) found in (8) can be most easily reduced by increasing either the drive displacement (X_D) or the sense-mode quality factor (Q_S), while the remaining parameters are generally fixed by the design. The sense-mode quality factor can be increased by operating the gyroscope in a vacuum ambient; however, once the operating ambient is sealed, it is not possible to increase the quality factor anymore. The only remaining parameter for reducing the noise-equivalent rate is then the drive-mode displacement amplitude, which can be increased easily by the amplitude control electronics in the *Drive Control Module*. From the readout electronics point of view, increasing the drive displacement also reduces the noise-equivalent readout noise since the scale factor directly depends on the drive displacement.

2) Test Results With Increased Drive Displacement: Increasing the drive displacement reduces the Brownian noise-equivalent rate as shown in (8); however, this also increases the quadrature signal, saturating the force-feedback electronics if not cancelled. The quadrature cancellation allows the gyroscope to operate with increased drive-displacement amplitudes. Table XII presents the performance results of the gyroscope with 3.5- and 7-μm drive displacements, both cases evaluated with and without the quadrature cancellation. It can be seen that some of the ARW data could not be measured without the quadrature cancellation due to the saturated force-feedback electronics as a result of high ZRO; however, it is possible to obtain the missing ARW data with the quadrature cancellation. From the test results in Table XII, it is clear that doubling the drive-displacement amplitude reduces the ARW or, equivalently, the gyro white noise by a factor of about two. In conclusion, the quadrature cancellation allows increasing the drive-displacement amplitude for a lower noise operation.

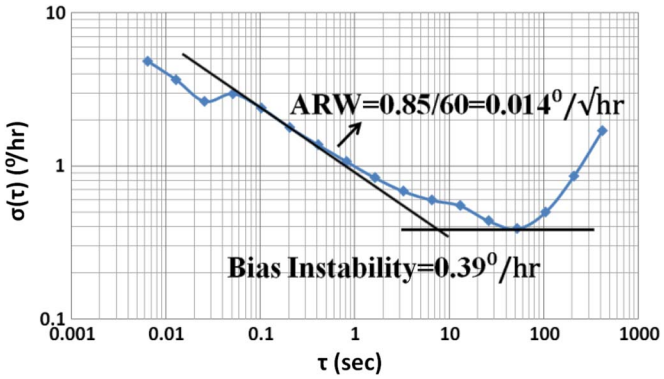

Fig. 12. Allan variance graph of Gyro#4 with exceptional performance, showing an exceptional bias instability of $0.39^\circ/\text{h}$ and ARW of $0.014^\circ/\sqrt{\text{h}}$. These results are achieved with the increased drive displacement (7 μm) and quadrature cancellation.

Fig. 12 shows the Allan variance graph of Gyro#4 in Table XII, illustrating an exceptional bias instability of $0.39^\circ/\text{h}$ and ARW of $0.014^\circ/\sqrt{\text{h}}$, where the latter is very close to the estimated ARW limit of $0.012^\circ/\sqrt{\text{h}}$. The result is obtained with the increased drive displacement of 7 μm and quadrature cancellation.

VI. CONCLUSION

This paper has provided a detailed analysis on the sources of the quadrature error and the effect of quadrature-error compensation on the gyro performance. FEM simulations have shown that rather than the mass and electrostatic-force imbalances, the imperfections in the mechanical elements that transmit motion or force between the modes cause a higher quadrature error. The force-transmitting elements should be designed more carefully to have the lowest possible quadrature error. The experimental investigation of the mechanical-spring imbalance in the tested fully decoupled gyroscopes has yielded a measured quadrature error up to $450^\circ/\text{s}$ with a 0.4-μm imbalance in the selected spring widths, in agreement with the $438^\circ/\text{s}$ quadrature error, which is predicted by the simulations.

Tests performed with and without the quadrature cancellation have shown that the bias instability and ARW performances of the gyroscopes improve up to an order of magnitude and that ZRO improves up to three orders of magnitude with the quadrature cancellation. In addition to these performance parameters, a significant improvement in the scale-factor repeatability and linearity has also been achieved with the quadrature cancellation by factors of about 4 and 20, respectively. A major improvement in the bias repeatability has not been observed with the quadrature cancellation, and this is believed to be due to the uncontrolled ambient-temperature variations during the bias-repeatability tests.

It is well known that increasing the drive displacement also increases the noise immunity of the gyroscope; however, the quadrature signal also grows up at the same time and saturates the angular-rate sensing electronics. With the quadrature cancellation, on the other hand, it has been experimentally shown that the fabricated gyroscopes can be operated with the increased drive displacement without saturating the electronics. Test results have verified that increasing the drive displacement has a direct effect on reducing ARW. A gyroscope with exceptional bias instability of $0.39^\circ/\text{h}$ and ARW of $0.014^\circ/\sqrt{\text{h}}$ is obtained with the quadrature cancellation and increased drive displacement. In summary, the cancellation of the quadrature error has been shown to have a significant role in the path to subdegree-per-hour inertial-grade MEMS gyroscopes.

ACKNOWLEDGMENT

The authors would like to thank M. Torunbalci and B. Eminoglu for their help during the fabrication and test of the gyroscopes.

REFERENCES

[1] B. R. Johnson, E. Cabuz, H. B. French, and R. Supino, "Development of a MEMS gyroscope for northfinding applications," in *Proc. PLANS*, Indian Wells, CA, May 2010, pp. 168–170.
[2] S. Niu and S. Gao, "Analysis of nonlinearities in force-to-voltage conversion in vibratory microgyroscope," in *Proc. ICMTMA*, Changsha, China, Mar. 2010, pp. 551–554.
[3] S. Iyer, Y. Zhou, and T. Mukherjee, "Analytical modeling of cross-axis coupling in micromechanical springs," in *Proc. Int. Conf. MSM*, Puerto Rico, Spain, Apr. 1999, pp. 632–635.
[4] J. A. Geen, "A path to low cost gyroscopy," in *Proc. Solid-State Sens., Actuators, Microsyst. Workshop*, Hilton Head Island, SC, Jun. 1998, pp. 51–54.
[5] R. Antonello, R. Oboe, L. Prandi, C. Caminada, and F. Biganzoli, "Open loop compensation of the quadrature error in MEMS vibrating gyroscopes," in *Proc. Ind. Electron. Conf.*, Porto, Portugal, Nov. 2009, pp. 4034–4039.
[6] M. Saukoski, L. Aaltonen, and K. A. I. Halonen, "Zero-rate output and quadrature compensation in vibratory MEMS gyroscopes," *IEEE Sens. J.*, vol. 7, no. 12, pp. 1639–1652, Dec. 2007.
[7] J. A. Geen, S. J. Sherman, J. F. Chang, and S. R. Lewis, "Single-chip surface micromachined integrated gyroscope with $50\ ^\circ/\text{h}$ Allan deviation," *IEEE J. Solid-State Circuits*, vol. 37, no. 12, pp. 1860–1866, Dec. 2002.
[8] J. A. Geen, "Micromachined gyros," U.S. Patent 6 122 961, Sep. 26, 2000.
[9] J. A. Geen, "Micromachined sensors with quadrature suppression," U.S. Patent 7 032 451, Apr. 25, 2006.
[10] J. Seeger, A. J. Rastegar, and M. T. Tormey, "Method and apparatus for electronic cancellation of quadrature error," U.S. Patent 0 180 908 A1, Aug. 9, 2007.
[11] W. A. Clark and R. T. Howe, "Surface micromachined z-axis vibratory rate gyroscope," in *Proc. Solid-State Sens., Actuators, Microsyst. Workshop*, Hilton Head Island, SC, Jun. 1996, pp. 283–287.
[12] A. Sharma, M. F. Zaman, and F. Ayazi, "A sub $0.2\ ^\circ/\text{hr}$ bias drift micromechanical gyroscope with automatic CMOS mode-matching," *IEEE J. of Solid-State Circuits*, vol. 44, no. 5, pp. 1593–1608, May 2009.
[13] B. Chaumet, B. Leverrier, C. Rougeot, and S. Bouyat, "A new silicon tuning fork gyroscope for aerospace applications," in *Proc. Symp. Gyro Technol.*, Karlsruhe, Germany, Sep. 2009, pp. 1.1–1.13.
[14] A. Sharma, M. F. Zaman, M. Zucher, and F. Ayazi, "A $0.1\ ^\circ/\text{hr}$ bias drift electronically matched tuning for microgyroscope," in *Proc. Int. Conf. MEMS*, Tucson, AZ, Jan. 2008, pp. 6–9.
[15] E. Tatar, S. E. Alper, and T. Akin, "Effect of quadrature error on the performance of a fully-decoupled MEMS gyroscope," in *Proc. Int. Conf. MEMS*, Cancun, Mexico, Jan. 2011, pp. 569–572.
[16] G. He and K. Najafi, "A single-crystal silicon vibrating ring gyroscope," in *Proc. Int. Conf. MEMS*, Las Vegas, NV, Jan. 2002, pp. 718–721.
[17] S. E. Alper, A. Aydemir, and T. Akin, "Stepped-etching for preserving critical dimensions in through-wafer deep reactive ion etching of thick silicon," in *Proc. 15th Int. Conf. TRANSDUCERS*, Denver, CO, Jun. 2009, pp. 1110–1113.
[18] T. B. Gabrielson, "Mechanical–thermal noise in micromachined acoustic and vibration sensors," *IEEE Trans. Electron Devices*, vol. 40, no. 5, pp. 903–909, May 1993.

Erdinc Tatar was born in Denizli, Turkey, in 1985. He received the B.S. and M.S. degrees (with high honors) in electrical and electronics engineering from Middle East Technical University (METU), Ankara, Turkey, in 2008 and 2010, respectively. He is currently working toward the Ph.D. degree in Electrical and Computer Engineering, Carnegie Mellon University, Pittsburgh, PA.

He was a Research Assistant with the Micro-Electro-Mechanical Systems Research and Applications Center, METU, between 2008 and 2011. He has been a Graduate Research Assistant with Carnegie Mellon University since 2012. His research interests include microelectromechanical systems gyroscopes, quadrature-error-reduction techniques, and analog closed-loop control.

Said Emre Alper (M'10) was born in Ankara, Turkey, in 1976. He received the B.S., M.Sc., and Ph.D. degrees (with high honors) in electrical and electronics engineering from Middle East Technical University (METU), Ankara, in 1998, 2000, and 2005, respectively.

From 1998 to 2005, he was a Research Assistant with the Microelectromechanical Systems (MEMS)-Very Large Scale Integrated Circuits Research Group, Department of Electrical and Electronics Engineering, METU, where he was a Senior Research Scientist and Instructor until 2008. Since 2008, he has continued research at the MEMS Research and Applications Center, METU, where he has been the Deputy Director since 2009 and also the Technical Leader of the Inertial Sensors Research and Technology Development Group. His major research interests include capacitive MEMS inertial sensors, capacitive interface circuits, analog closed-loop control, various microfabrication technologies, packaging and testing of MEMS inertial sensors, and also hybrid system design.

Dr. Alper was the recipient of the "METU Thesis of the Year Award" in 2000 and 2005 for his M.Sc. thesis and Ph.D. dissertation, respectively, which were awarded by the Prof. Mustafa N. Parlar Education and Research Foundation. He is the first author of the symmetric and decoupled gyroscope design, which won the first-prize award in the operational designs category of the "International Design Contest" organized by the Design, Automation, and Test Conference in Europe and Circuits Multi-Projets (CMP) in March 2001. He is also the first author of the tactical-grade symmetrical and decoupled microgyroscope design, which won the third-prize award, among 132 MEMS designs from 24 countries and 25 states across the U.S., in the international "3-D MEMS Design Challenge" organized by MEMGen Corporation (currently Microfabrica, Inc.) in June 2003.

Tayfun Akin was born in Van, Turkey, in 1966. He received the B.S. degree (with high honors) in electrical engineering from Middle East Technical University (METU), Ankara, Turkey, in 1987, and the M.S. and Ph.D. degrees in electrical engineering from the University of Michigan, Ann Arbor, in 1989 and 1994, respectively, with a graduate fellowship provided by the NATO Science Scholarship Program through the Scientific and Technical Research Council of Turkey (TUBITAK).

Since 1995, 1998, and 2004, he has been an Assistant Professor, Associate Professor, and Professor, respectively, with the Department of Electrical and Electronics Engineering, METU. He is also the Director of the Micro-Electro-Mechanical Systems Research and Applications Center, METU, which has a 1300-m^2 clean-room area for microelectromechanical systems (MEMS) process and testing. His research interests include MEMS, microsystems technologies, infrared detectors and readout circuits, silicon-based integrated sensors and transducers, and analog and digital integrated-circuit design.

Dr. Akin has served various MEMS, EUROSENSORS, and TRANSDUCERS conferences as a Technical Program Committee Member. He was the Co-Chair of the 19th IEEE International Conference of Micro Electro Mechanical Systems (MEMS 2006) held in Istanbul, and he was the Co-Chair of the Steering Committee of the IEEE MEMS Conference in 2007. He was the recipient of the First Prize in the Experienced Analog/Digital Mixed-Signal Design Category at the 1994 Student Very Large Scale Integrated Circuit Design Contest organized and sponsored by Mentor Graphics, Texas Instruments, Hewlett–Packard, Sun Microsystems, and *Electronic Design Magazine*. He is the coauthor of the symmetric and decoupled gyroscope project which won the first-prize award in the operational designs category of the international design contest organized by Design, Automation, and Test Conference and Circuits Multi-Projets (CMP) in March 2001. He is also the coauthor of the gyroscope project which won the third-prize award of the 3-D MEMS Design Challenge organized by MEMGen Corporation (currently Microfabrica, Inc.).